

## High-pressure synthesis of skiaigite-majorite garnet and investigation of its crystal structure

LEYLA ISMAILOVA<sup>1,2,\*</sup>, ANDREY BOBROV<sup>3</sup>, MAXIM BYKOV<sup>1</sup>, ELENA BYKOVA<sup>1,2</sup>, VALERIO CERANTOLA<sup>2</sup>,  
INNOKENTY KANTOR<sup>4</sup>, ILYA KUPENKO<sup>4</sup>, CATHERINE MCCAMMON<sup>2</sup>, VADIM DYADKIN<sup>4</sup>,  
DMITRY CHERNYSHOV<sup>4</sup>, SAKURA PASCARELLI<sup>4</sup>, ALEXSANDR CHUMAKOV<sup>4</sup>, NATALIA DUBROVINSKAIA<sup>1</sup>  
AND LEONID DUBROVINSKY<sup>2</sup>

<sup>1</sup>Laboratory of Crystallography, Universität Bayreuth, 95447 Bayreuth, Germany

<sup>2</sup>Bayerisches Geoinstitut, Universität Bayreuth, 95447 Bayreuth, Germany

<sup>3</sup>Department of Petrology, Geological Faculty, Moscow State University, 119234 Moscow, Russia

<sup>4</sup>ESRF, European Synchrotron Radiation Facility, CS40220 38043 Grenoble Cedex 9, France

### ABSTRACT

Skiagite-rich garnet was synthesized as single crystals at 9.5 GPa and 1100 °C using a multi-anvil apparatus. The crystal structure [cubic, space group  $Ia\bar{3}d$ ,  $a = 11.7511(2)$  Å,  $V = 1622.69(5)$  Å<sup>3</sup>,  $D_{\text{calc}} = 4.4931$  g/cm<sup>3</sup>] was investigated using single-crystal synchrotron X-ray diffraction. Synchrotron Mössbauer source spectroscopy revealed that Fe<sup>2+</sup> and Fe<sup>3+</sup> predominantly occupy dodecahedral (X) and octahedral (Y) sites, respectively, as expected for the garnet structure, and confirmed independently using nuclear forward scattering. Single-crystal X-ray diffraction suggests the structural formula of the skiaigite-rich garnet to be  $\text{Fe}_3^{2+}(\text{Fe}_{0.234(2)}^{2+}\text{Fe}_{1.532(1)}^{3+}\text{Si}_{0.234(2)}^{4+})(\text{SiO}_4)_3$ , in agreement with electron microprobe chemical analysis. The formula is consistent with X-ray absorption near-edge structure spectra. The occurrence of Si and Fe<sup>2+</sup> in the octahedral Y-site indicates the synthesized garnet to be a solid solution of end-member skiaigite with ~23 mol% of the Fe-majorite end-member  $\text{Fe}_3^{2+}(\text{Fe}^{2+}\text{Si}^{4+})(\text{SiO}_4)_3$ .

**Keywords:** Skiagite, majorite, garnets, single-crystal X-ray diffraction, Mössbauer spectroscopy, nuclear forward scattering, XANES

### INTRODUCTION

Garnet is a common mineral in mantle assemblages and often occurs as inclusions in natural diamonds. Due to the compositional complexity of natural garnets, the relationship between their composition and the pressure-temperature conditions of their formation is still not well constrained (Akaogi and Akimoto 1977; Irifune 1987; Stachel 2001; Collerson et al. 2010).

Silicate garnets have the general formula  $[\text{X}]_3[\text{Y}]_2\text{Si}_3\text{O}_{12}$  where [X] and [Y] are cations occupying the dodecahedral and octahedral sites, respectively. In garnets from the crust and upper mantle the dodecahedral site is occupied by a divalent cation (e.g., Fe<sup>2+</sup>, Mg<sup>2+</sup>, Ca<sup>2+</sup>) and the octahedral site by a trivalent cation (e.g., Fe<sup>3+</sup>, Al<sup>3+</sup>, Cr<sup>3+</sup>). Garnets from mantle xenoliths and inclusions in diamonds contain both ferrous (Fe<sup>2+</sup>) and ferric (Fe<sup>3+</sup>) iron. Thus information about the properties and high-pressure behavior of the iron end-member skiaigite,  $\text{Fe}_3^{2+}\text{Fe}_3^{3+}(\text{SiO}_4)_3$ , is important for mineral physics and the geochemistry of the Earth's upper mantle and transition zone. Moreover, the fate of iron-rich silicate material incorporating a skiaigite component is unknown at conditions of the deep lower mantle and the core-mantle boundary.

The stability field of skiaigite has been investigated in several studies. Karpinskaya et al. (1982) were probably the first to synthesize skiaigite, which was produced at 12 GPa and 800 °C. Woodland and O'Neill (1993) measured the variation of garnet unit-cell parameter along the almandine-skiagite solid solution join. Woodland and Ross (1994) studied the crystal chemistry of skiaigite solid solutions along the joins  $\text{Fe}_3\text{Al}_2(\text{SiO}_4)_3$ –

$\text{Fe}_3\text{Fe}_2(\text{SiO}_4)_3$  (almandine-skiagite) and  $\text{Ca}_3\text{Fe}_2(\text{SiO}_4)_3$ – $\text{Fe}_3\text{Fe}_2(\text{SiO}_4)_3$  (andradite-skiagite) at pressures between 1.7 and 9.7 GPa and temperatures of 1080 to 1100 °C. Woodland and O'Neill (1995) investigated the stability of Ca-bearing garnets on the join  $\text{Ca}_3\text{Fe}_2(\text{SiO}_4)_3$ – $\text{Fe}_3\text{Fe}_2(\text{SiO}_4)_3$  (andradite-skiagite) as a function of pressure at 1100 °C. Simple Cr<sup>3+</sup>–Fe<sup>3+</sup> exchange in the octahedral sites of the skiaigite–Fe-knorringite [ $\text{Fe}_3\text{Fe}_2(\text{SiO}_4)_3$ – $\text{Fe}_3\text{Cr}_2(\text{SiO}_4)_3$ ] binary join was studied by Woodland et al. (2009). However, so far the iron-skiagite end-member has not yet been synthesized so that it can be investigated by mineral physics methods, including single-crystal X-ray diffraction and Mössbauer spectroscopy.

Here we report the high-pressure high-temperature synthesis of single crystals of skiaigite-rich garnet,  $\text{Fe}_3^{2+}(\text{Fe}_{0.234(2)}^{2+}\text{Fe}_{1.53(1)}^{3+}\text{Si}_{0.234(2)}^{4+})(\text{SiO}_4)_3$ , and the results of its characterization using single-crystal synchrotron X-ray diffraction, synchrotron Mössbauer source (SMS) spectroscopy, nuclear forward scattering (NFS), and X-ray absorption near-edge structure (XANES) spectroscopies.

### EXPERIMENTAL METHODS

Synthesis experiments were performed using a split-sphere type multi-anvil apparatus at 9.5 GPa and 1100 °C at Bayerisches Geoinstitut (Bayreuth, Germany) (BGI). The starting material (corresponding to the nominal composition  $\text{Fe}_3\text{Fe}_2\text{Si}_3\text{O}_{12}$ ) was a powdered mixture of chemically pure oxides ( $\text{Fe}_{1-x}\text{O}$ ,  $^{57}\text{Fe}_2\text{O}_3$ , and  $\text{SiO}_2$ ) homogenized at room temperature by milling in a mortar using ethanol and then dried in a furnace at 100 °C for 24 h. The prepared mixture was placed in a capsule of 3.5 mm length and 2 mm diameter made of platinum foil. High temperature was generated using a LaCrO<sub>3</sub> heater and the capsule was insulated from the heater by a MgO cylinder. The cell assembly with the sample was compressed to the target pressure between eight cubic tungsten carbide anvils with corners truncated to 11.0 mm edge lengths. The accuracy in determination of pressure and temperature is estimated to be ±0.5 GPa and ±50 °C, respectively (Frost et al. 2004).

\* E-mail: leyla.isml@gmail.com

The sample was heated for about 30 min and rapidly quenched by switching off the power supply, causing cooling to ambient temperature with a rate of  $\sim 200$  °C/s.

Chemical composition of the samples was characterized using wavelength-dispersive X-ray (WDX) microprobe analysis (JEOL JXA-8200; focused beam; accelerating voltage of 15 keV and beam current of 15 nA). Metallic Fe and quartz were used as standards for Fe and Si, respectively, with atomic number effects, absorption, and fluorescence (ZAF) correction.

SMS spectra were recorded at the Nuclear Resonance Beamline (Rüffer and Chumakov 1996) ID18 of the European Synchrotron Radiation Facility (ESRF) (Grenoble, France) using the (111) Bragg reflection of a  $^{57}\text{FeBO}_3$  single crystal mounted on a Wissel velocity transducer driven with a sinusoidal wave form (Potapkin et al. 2012). The X-ray beam was focused to 20  $\mu\text{m}$  vertical and 10  $\mu\text{m}$  horizontal dimensions using Kirkpatrick-Baez mirrors. The line width of the SMS and the absolute position of the center shift (CS) were controlled before and after each measurement using a  $\text{K}_2\text{Mg}^{57}\text{Fe}(\text{CN})_6$  reference single line absorber. The velocity scale was calibrated using 25  $\mu\text{m}$  thick natural  $\alpha$ -Fe foil. Each spectrum took  $\sim 1$ –2 h to collect. Spectra were fitted using a full transmission integral with a normalized Lorentzian-squared source lineshape using the MossA software package (Prescher et al. 2012).

NFS data were collected at the same beamline in 4-bunch mode, with the beam focused to  $6 \times 11$   $\mu\text{m}^2$  using Kirkpatrick-Baez mirrors. The spectra were collected for 10 to 60 min each. NFS data were fitted using the CONUSS package (Sturhahn 2000).

XANES spectra were collected at the energy-dispersive X-ray absorption spectroscopy beamline (ID24) at ESRF. The beam was focused horizontally using a curved polychromator Si (111) crystal in Bragg geometry and vertically with Kirkpatrick-Baez (KB) mirrors. The size of the X-ray beam spot on the sample was about  $3.5 \times 5$   $\mu\text{m}^2$  FWHM. The measured XANES spectra were normalized using FDMNES software (Bunau and Joly 2009). The second-order polynomial pixel to energy conversion parameters were calibrated using a reference  $\alpha$ -Fe foil. Crystals for all studies were selected at BGI using a three-circle Bruker diffractometer equipped with a SMART APEX CCD detector and a high-brilliance Rigaku diffractometer equipped with a rotating anode (Rotor Flex FR-D, MoK $\alpha$  radiation), Osmic focusing X-ray optics, and Bruker Apex CCD detector.

Single-crystal X-ray diffraction data were collected at the Swiss-Norwegian beamline (BM01A) at ESRF on a single-crystal diffractometer (KUMA KM6-CH) by  $360^\circ \phi$  scans ( $\Delta\phi = 0.5^\circ$ ) employing a Pilatus 2M pixel detector. The crystal was cooled to 280 K using an Oxford Cryostream low-temperature device. Data processing (peak intensity integration, background evaluation, cell parameters, space group determination, and absorption correction) was performed with the CrysAlis Pro 171.36.28 program. The program JANA2006 was used for structure refinement (Petricek et al. 2014).

## RESULTS AND DISCUSSION

### Phase assemblage and chemical composition

The recovered sample is a multi-phase assemblage that includes fine anhedral garnet crystals that appear red under a light microscope and typically have dimensions less than  $30 \times 10 \times 10$   $\mu\text{m}^3$ . There are also minor amounts of magnetite, coesite, and clinopyroxene (Fig. 1) that were confirmed by X-ray diffraction data and microprobe analysis. The presence of other phases in addition to garnet may indicate a non-homogeneous pressure-temperature distribution within the pressure chamber and/or different kinetics of chemical reactions in the starting mixture.

The composition of skiagite garnet was obtained by averaging 30 microprobe analyses (in wt% with standard deviations given in parentheses):  $\text{SiO}_2$  35.21(11),  $\text{FeO}$  60.67(9), total 95.88(14), which led to a chemical formula of  $\text{Fe}_{0.276(1)}^{2+}(\text{Fe}_{0.276(1)}^{2+}\text{Si}_{0.276(1)})\text{Si}_3\text{O}_{12}$  on the basis of 12 oxygen atoms assuming stoichiometry and that the dodecahedral position is occupied exclusively by  $\text{Fe}^{2+}$ . The  $\text{Fe}^{3+}$ -corrected values of the microprobe analyses are (in wt%):  $\text{SiO}_2$  35.21(11),  $\text{FeO}$  42.11(36),  $\text{Fe}_2\text{O}_3$  20.63(80), total 97.95(88). No chemical zoning was observed in the run products. As evident from the formula, there is an excess of Si over the ideal three atoms per formula unit.

### Single-crystal X-ray diffraction and structure refinement

The experimental details and crystallographic data obtained by means of synchrotron X-ray diffraction from a small (red) crystal of skiagite garnet are summarized in Table 1. Fractional atomic coordinates and isotropic or equivalent isotropic displacement parameters ( $\text{\AA}^2$ ), atomic displacement parameters ( $\text{\AA}^2$ ), selected geometric parameters (in angstroms and degrees) are listed in Tables 2–4. (CIF<sup>1</sup> is available.) Full-matrix least-squares refinement on  $F$  provided good reliability factors  $R_F[I > 3\sigma(I)] = 0.0281$  and  $wR_F(\text{all}) = 0.0427$ . Atomic coordinates and anisotropic displacement parameters of Fe1 and Si1 were constrained to be equal, and their overall occupancy was fixed. Structure refinement revealed that the octahedral site is fully occupied by

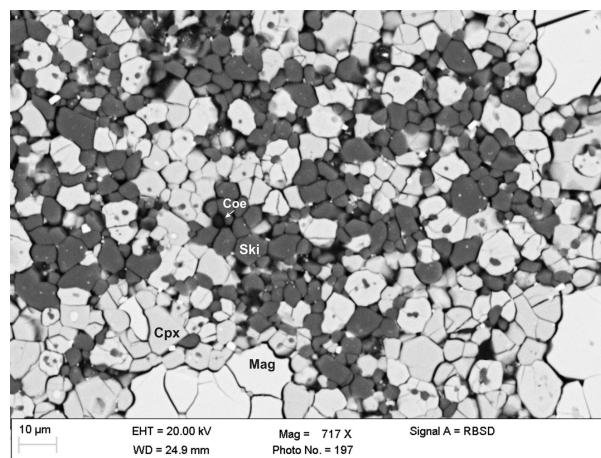


**FIGURE 1.** Backscattered electron image of the sample (S5962) synthesized at 9.5 GPa and 1100 °C consisting of skiagite-rich garnet (Ski = gray), clinopyroxene (Cpx = light gray), coesite (Coe = black), and magnetite (Mag = white).

**TABLE 1.** Crystal data and structure refinement

Chemical formula	$\text{Fe}_{0.276}^{2+}(\text{Fe}_{0.276}^{2+}\text{Si}_{0.276})\text{Si}_3\text{O}_{12}$
Formula weight (g/mol)	548.98
Crystal system, space group	Cubic, $Im\bar{3}d$
Temperature (K)	280.0(1)
$a$ ( $\text{\AA}$ )	11.7511(2)
$V$ ( $\text{\AA}^3$ )	1622.69(5)
$Z$	8
Radiation type	Synchrotron, $\lambda = 0.6946$ $\text{\AA}$
$\mu$ ( $\text{mm}^{-1}$ )	10.997
Crystal size (mm)	$0.02 \times 0.019 \times 0.01$
Density (calculated)	4.494 g/cm <sup>3</sup>
<b>Data collection</b>	
Absorption correction	Multi-scan (SCALE3 ABSPACK)
$T_{\text{min}}, T_{\text{max}}$	0.730, 1
No. of measured, independent, and observed [ $I > 3\sigma(I)$ ] reflections	5517, 255, 215
$R_{\text{int}}$	0.028
$(\sin \theta/\lambda)_{\text{max}}$ ( $\text{\AA}^{-1}$ )	0.763
<b>Refinement</b>	
$R_F$ [ $I > 3\sigma(I)$ ], $wR(\text{all})$ , $S$	0.028, 0.043, 2.33
No. of reflections	255
No. of parameters	18
$\Delta\rho_{\text{max}}, \Delta\rho_{\text{min}}$ ( $\text{e}\text{\AA}^{-3}$ )	0.63, -0.69

<sup>1</sup> Deposit item AM-15-115278, CIF. Deposit items are free to all readers and found on the MSA web site, via the specific issue's Table of Contents (go to <http://www.minsocam.org/MSA/AmMin/TOC/>).

Fe and Si atoms, yielding the chemical composition  $\text{Fe}_3^{2+}(\text{Fe}_{0.234(2)}^{2+}\text{Fe}_{1.532(1)}^{3+}\text{Si}_{0.234(2)}^{4+})(\text{SiO}_4)_3$ , which is in good agreement with the results of electron microprobe analysis. The minor difference in the chemical composition determined by these two methods is likely due to the bulk averaging of the microprobe data compared to the diffraction data that measures a single crystal; therefore the values obtained from single-crystal X-ray diffraction are considered to be more representative. According to the obtained structural formula, there is a significant amount of Si [0.234(2)] and  $\text{Fe}^{2+}$  [0.234(2)] on the octahedral position. This suggests that ~23 mol% of the end-member iron-majorite ( $\text{Fe}_4\text{Si}_4\text{O}_{12}$ ) component is present in the synthesized skiagite-rich garnet.

### Mössbauer spectroscopy and nuclear forward scattering

Skiagite-rich garnet crystals, identified using single-crystal X-ray diffraction, were loaded into a DAC and studied at ambient pressure. We collected SMS spectra from several crystals and fit them to doublets with conventional constraints (equal doublet component widths and areas). All spectra gave hyperfine parameters that were the same within experimental uncertainty with the exception of relative intensities of the different doublets. This difference likely arises from varying ratios of different iron isotopes due to the starting mixture containing unenriched  $\text{Fe}_{1-x}\text{O}$  and  $^{57}\text{Fe}$ -enriched  $\text{Fe}_2\text{O}_3$ , where partial isotopic differentiation occurred in the course of the chemical reaction.

A typical SMS spectrum of skiagite-rich garnet contains two doublets (Fig. 2) that according to literature data (Amthauer et al. 1976; Woodland and Ross 1994) can be assigned to  $\text{Fe}^{2+}$  on the dodecahedral site and  $\text{Fe}^{3+}$  on the octahedral site. Some of the crystals showed an additional doublet consistent with  $\text{Fe}^{2+}$  on

the octahedral site, although with low intensity likely due to the isotopic effect mentioned above. The NFS spectrum collected at ambient conditions (Fig. 3) is consistent with the SMS spectrum and the fit gave similar hyperfine parameters (Table 5). Since the absolute CS value cannot be determined from the NFS data, it was fixed to the value determined from the SMS spectrum.

### XANES

XANES spectra were simulated using ab initio multiple scattering calculations with the FEFF9 code (Rehr et al. 2009; Pascarelli et al. 2006). The atomic clusters for Fe1 and Fe2 positions were calculated from the structural model obtained in the single-crystal X-ray diffraction study. Full multiple scattering calculations were performed in a 6 Å radius cluster, while self-consistent potentials were calculated for a 4 Å radius cluster. The Hedin-Lundqvist self-energy exchange correlation was used and multipole (dipole + quadrupole) transitions were calculated to simulate the pre-edge transition peak.

Figure 4 shows the experimental XANES spectra of skiagite-

**TABLE 2.** Fractional atomic coordinates and equivalent isotropic ( $U_{\text{eq}}$ ) displacement parameters ( $\text{\AA}^2$ )

	X	Y	Z	$U_{\text{eq}}$	Occupancy
Fe2	1/2	0	1/4	0.0122(2)	0.883(7)
Fe1	0	0	0	0.0077(2)	
Si2	3/4	0	1/4	0.0085(3)	0.117(7)
O1	0.03501(15)	0.05281(15)	0.65693(15)	0.0112(5)	
Si1	0	0	0	0.0077(2)	

**TABLE 3.** Atomic displacement parameters ( $\text{\AA}^2$ )

	$U^{11}$	$U^{22}$	$U^{33}$	$U^{12}$	$U^{13}$	$U^{23}$
Fe2	0.0081(4)	0.0143(3)	0.0143(3)	0	0	0.0012(3)
Fe1	0.0077(4)	0.0077(4)	0.0077(4)	0.00007(17)	0.00007(17)	0.00007(17)
Si2	0.0072(6)	0.0092(4)	0.0092(4)	0	0	0
O1	0.0109(8)	0.0126(8)	0.0100(8)	0.0010(7)	-0.0007(7)	-0.0001(6)
Si1	0.0077(4)	0.0077(4)	0.0077(4)	0.00007(17)	0.00007(17)	0.00007(17)

**TABLE 4.** Selected geometric parameters: interatomic distances ( $\text{\AA}$ ), bond angles in degrees

Fe2-Fe1	3.2845(19)	Fe2-O1 <sup>ii</sup>	2.3831(17)
Fe2-Si2	2.9378(10)	Fe1-O1 <sup>iii</sup>	1.9888(17)
Fe2-O1 <sup>i</sup>	2.2620(18)	Si2-O1 <sup>i</sup>	1.6430(18)
O1 <sup>iv</sup> -Fe2-O1 <sup>i</sup>	115.19(6)	O1 <sup>iv</sup> -Fe2-O1 <sup>viii</sup>	123.62(6)
O1 <sup>iv</sup> -Fe2-O1 <sup>i</sup>	71.69(6)	O1 <sup>i</sup> -Fe2-O1 <sup>ii</sup>	73.03(6)
O1 <sup>iv</sup> -Fe2-O1 <sup>ii</sup>	111.13(6)	O1 <sup>viii</sup> -Fe2-O1 <sup>ii</sup>	161.88(6)
O1 <sup>iv</sup> -Fe2-O1 <sup>i</sup>	93.00(6)	O1 <sup>iv</sup> -Fe1-O1 <sup>iii</sup>	91.89(7)
O1 <sup>iv</sup> -Fe2-O1 <sup>iii</sup>	71.89(6)	O1 <sup>iv</sup> -Fe1-O1 <sup>xi</sup>	88.11(7)
O1 <sup>viii</sup> -Fe2-O1 <sup>i</sup>	67.55(6)	O1 <sup>xi</sup> -Fe1-O1 <sup>iii</sup>	180.0(5)
O1 <sup>viii</sup> -Fe2-O1 <sup>viii</sup>	73.03(6)	O1 <sup>viii</sup> -Si2-O1 <sup>i</sup>	114.47(9)
O1 <sup>viii</sup> -Fe2-O1 <sup>ii</sup>	123.62(6)	O1 <sup>viii</sup> -Si2-O1 <sup>i</sup>	99.87(9)

Notes: Symmetry code(s): (i)  $x+1/4, z-3/4, y+1/4$ ; (ii)  $-z+3/4, y-1/4, -x+1/4$ ; (iii)  $y, z-1/2, -x$ ; (iv)  $-x, -y, -z+1$ ; (v)  $z-1/2, x, -y+1/2$ ; (vi)  $z-1/2, -x, y$ ; (vii)  $x+1/4, -z+3/4, -y+1/4$ ; (viii)  $-z+3/4, -y+1/4, x+1/4$ ; (ix)  $x, -y, -z+1/2$ ; (x)  $-z+1/2, x, -y$ ; (xi)  $-y, -z+1/2, x$ ; (xii)  $-x+1/2, -y, z-1/2$ .

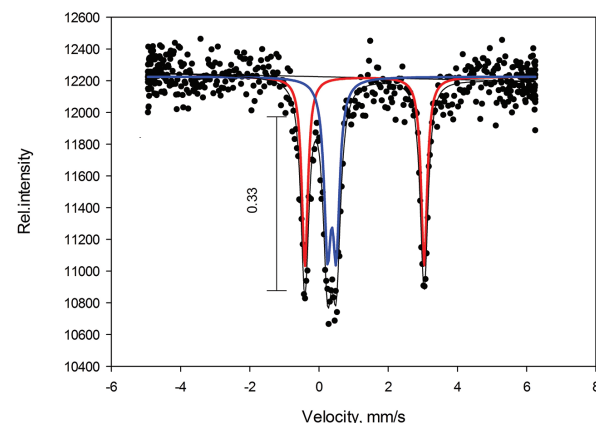


**FIGURE 2.**  $^{57}\text{Fe}$  SMS spectrum of skiagite-rich garnet at ambient conditions. The solid line shows the fit with parameters given in Table 5. Red and blue doublets represent  $\text{Fe}^{2+}$  and  $\text{Fe}^{3+}$ , respectively. (Color online.)

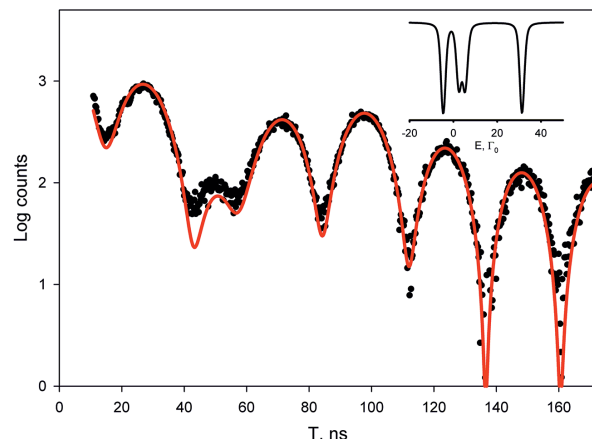


**FIGURE 3.** NFS spectrum of skiagite-rich garnet at ambient conditions. The solid line shows the fit with parameters given in Table 5. The inset shows the energy domain spectrum represented by the time domain data. (Color online.)

**TABLE 5.** Hyperfine parameters of skiaigite-rich garnet at ambient conditions

Oxidation state	Position	Center shift (CS) <sup>a</sup> (mm/s)	Quadrupole splitting (QS) (mm/s)	FWHM (mm/s)
<b>SMS spectroscopy</b>				
Fe <sup>2+</sup>	Dodecahedral	1.31(1)	3.45(2)	0.15(3)
Fe <sup>3+</sup>	Octahedral	0.37(1)	0.26(2)	0.19(4)
<b>NFS spectroscopy</b>				
Fe <sup>2+</sup>	Dodecahedral	1.31 <sup>b</sup>	3.49(5)	
Fe <sup>3+</sup>	Octahedral	0.40(5)	0.27(1)	

<sup>a</sup> Relative to  $\alpha$ -Fe.<sup>b</sup> Fixed to value from SMS.

rich garnet and simulated XANES spectra for the adopted structural model. Energies of simulated spectra were shifted so as to fit each simulated curve to the corresponding observed spectra.

Each spectrum is characterized by two parts: a pre-edge region ( $\sim 7113$  eV) and a main-edge region (7120–7150 eV). Because skiaigite-rich garnet is cubic, there is no linear polarization effect and spectra are the same for any crystal orientation. Our experimental setup at the beamline did not allow the collection of spectra with sufficient quality in the pre-edge region. However, comparison of the main-edge regions suggests that the simulated spectra are representative of the experimental ones.

### Comparison of the crystal structures of Fe-bearing garnet end-members

The most abundant end-members of Fe-bearing garnets are almandine,  $\text{Fe}^{3+}\text{Al}_2\text{Si}_2\text{O}_{12}$ , and andradite,  $\text{Ca}_3\text{Fe}^{3+}(\text{SiO}_4)_3$ , which are stable at ambient pressure. Knorringite,  $\text{Fe}_3\text{Cr}_2\text{Si}_3\text{O}_{12}$ , is stable above 6 GPa (Fursenko 1981). Majorite,  $\text{Mg}_3(\text{Fe}^{2+}\text{Si})(\text{SiO}_4)_3$ , is considered to be an abundant garnet component at depths  $>350$  km (Ringwood 1975). All of the end-members form solid solutions with skiaigite (Fig. 5).

Woodland and Ross (1994) carried out a single-crystal X-ray diffraction study of two almandine-skiagite and five andradite-skiagite crystals to investigate variations in bond length with increasing skiaigite content. In andradite-skiagite solid solutions  $\text{Fe}^{2+}$  substitutes for the larger  $\text{Ca}^{2+}$  on the dodecahedral sites, so that an increase of the skiaigite-component leads to shortening of average  $[(\text{Fe}^{2+}, \text{Ca})\text{O}]_1$  and  $[(\text{Fe}^{2+}, \text{Ca})\text{O}]_2$  bond lengths. Since six of the 12 octahedral edges are shared with neighboring dodecahedra, the octahedral Fe–O bond lengths also shorten. In almandine-skiagite solid solutions an increase of the skiaigite-component means that  $\text{Al}^{3+}$  is substituted by larger  $\text{Fe}^{3+}$  cations on octahedral sites that results in an increase of the cation-oxygen octahedral  $[(\text{Fe}^{3+}, \text{Al})\text{O}]$  bond lengths, whereas the lengths of the two non-equivalent dodecahedral bonds (Fe–O)<sub>1</sub> and (Fe–O)<sub>2</sub> remain almost constant (Fig. 6).

The tetrahedral (Si–O) bond lengths remain constant across all joins and undergo only minor changes of  $\sim 0.005$  Å in almandine-skiagite garnets and  $\sim 0.01$  Å in andradite-skiagite garnets. The change in Si–O bond lengths along the andradite-skiagite join is likely a response to the large decrease in the volume of neighboring dodecahedra, which leads to a slight distortion of tetrahedra.

### Majoritic component in synthetic garnets

Iron majorite (Fe-maj,  $\text{Fe}_4\text{Si}_4\text{O}_{12}$ ) is the hypothetical end-member of iron-bearing, high-pressure garnets. As demonstrated by Akaogi and Akimoto (1977), the solubility of iron majorite in almandine reaches a maximum of 40 mol% between 9.0 and 10.0

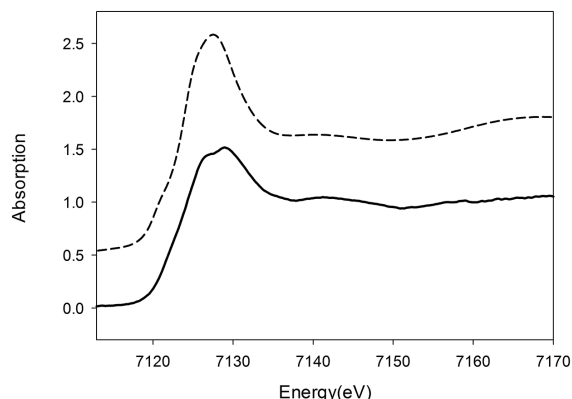


**FIGURE 4.** Normalized Fe *K*-edge XANES spectra (solid line = experimental and dashed line = simulated) of skiaigite-rich garnet at ambient conditions.

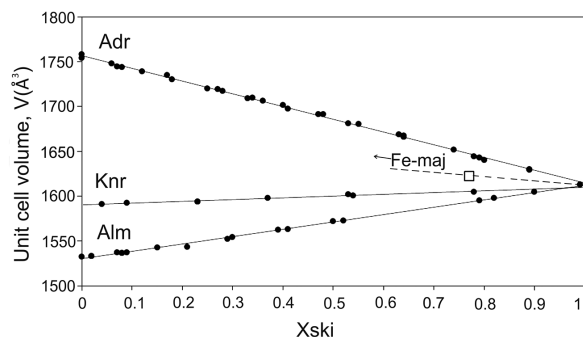


**FIGURE 5.** Unit-cell volume,  $V$ , plotted as a function of the skiaigite content in andradite-skiagite, almandine-skiagite, and knorringite-skiagite solid solutions. Data for almandine-skiagite and andradite-skiagite are from Woodland and Ross (1994), and for knorringite-skiagite from Woodland et al. (2009). The open square indicates the skiaigite-majorite solid solution from this study. Uncertainties are less than the size of the symbols.

GPa at 1000 °C. They estimated a unit-cell parameter of 11.595 Å ( $V = 1558.89$  Å<sup>3</sup>) for the  $\text{Fe}_4^{2+}\text{Si}_4\text{O}_{12}$  end-member by extrapolation.

The solubility of the iron majorite component in skiaigite has not been previously demonstrated. Woodland and O'Neill (1993) showed that no significant excess of silicon ( $>3$  cations pfu) was detected in garnet synthesized at 10 GPa and 1100 °C from a starting material with 60% skiaigite and 40% majorite. This was confirmed by the observed cell parameter that did not deviate from that of pure skiaigite ( $a = 11.7286$  Å) (Woodland and O'Neill 1993).

The structural formula obtained from EMPA and single-crystal X-ray diffraction data shows that the skiaigite-rich garnet synthesized in our experiment contains excess Si and  $\text{Fe}^{2+}$  entering the Y site. The cell parameter of this garnet is higher [ $a = 11.7511(2)$  Å] compared to the one ( $a = 11.7286$  Å) reported by Woodland and O'Neill (1993) for pure skiaigite. This can be explained by incorporation of the iron majorite component (23 mol%  $\text{Fe}_4\text{Si}_4\text{O}_{12}$ ) into skiaigite due to the reaction  $\text{Fe}_3^{3+}\text{Fe}_3^{3+}\text{Si}_3\text{O}_{12} = 2\text{Fe}^{2+}\text{SiO}_3 + \text{Fe}^{2+}\text{Fe}_2^{3+}\text{O}_4 + \text{SiO}_2$ . Additionally, our structural data provide evidence for increase of the unit-cell parameter from skiaigite to iron majorite (dashed line in Fig. 6). If the data are linearly extrapolated (Fig.



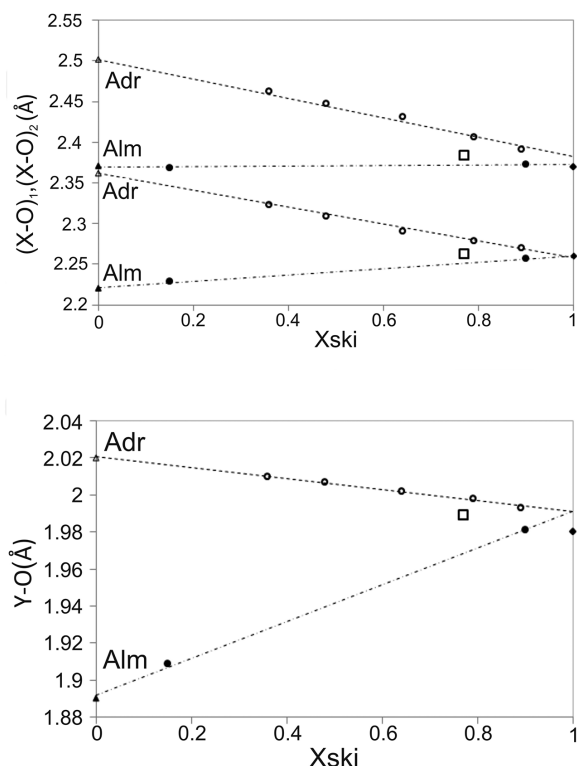


**FIGURE 6.** Variation of the X-O and Y-O bonds lengths with the proportion of skiagite-component in andradite-skiagite and almandine-skiagite solid solutions [X and Y indicate cations in dodecahedral (X) and octahedral (Y) sites] after Woodland and Ross (1994). Data for the andradite (solid triangles) and almandine (opened triangles) end-members are from Armbruster et al. (1992) and Armbruster and Geiger (1993). Open squares indicate the skiagite-majorite garnet from this study.

6), the unit-cell parameter of iron majorite in our study is found to be  $a = 11.833 \text{ \AA}$ , which is higher than the value obtained by Akaogi and Akimoto (1977) ( $a = 11.595 \text{ \AA}$ ) through extrapolation of iron majorite–almandine solubility data.

### IMPLICATIONS

The results of our study provide information on the solubility of the iron-majorite end-member in skiagite. We have demonstrated the possibility to synthesize high-quality single crystals of majorite-skiagite garnet and through single-crystal X-ray diffraction data revealed that at least 23 mol% of iron-majorite can be dissolved in skiagite at high-pressure and high-temperature conditions. The studied garnet contains octahedral Si, which can be an important pressure indicator for garnets in mantle assemblages (Akaogi and Akimoto 1977). The relationship between skiagite and majorite provides evidence for similarity in their crystal-chemical behavior, but, at the same time, suggests a consequent reaction on pressure increase. Although both are high-pressure components of garnet, the proportion of iron majorite component relative to skiagite should decrease with increasing pressure. Our data motivates a detailed investigation of structural changes in the skiagite–majorite series as a function of pressure and temperature.

### ACKNOWLEDGMENTS

This study was partly supported by the Russian Foundation for Basic Research (project no. 15-05-08261 to Leyla Ismailova and Andrey Bobrov). Natalia Dubrovinskaya and Leonid Dubrovinsky thank Deutsche Forschungsgemeinschaft (DFG) and the Federal Ministry of Education and Research (BMBF), Germany, for financial support. We acknowledge the European Radiation Facility for provision of synchrotron radiation facilities (BM01 SNBL, ID18, ID24). We thank U. Trenz and D. Krause for support during the SEM and microprobe measurements.

### REFERENCES CITED

- Akaogi, M., and Akimoto, A. (1977) Pyroxene-garnet solid-solution equilibria in the system  $\text{Mg}_2\text{Si}_4\text{O}_{12}$ – $\text{Mg}_3\text{Al}_2\text{Si}_2\text{O}_{12}$  and  $\text{Fe}_3\text{Al}_2\text{Si}_2\text{O}_{12}$ – $\text{Fe}_2\text{Al}_2\text{Si}_2\text{O}_{12}$  at high pressures and temperatures. *Physics of the Earth and Planetary Interiors*, 111, 90–106.
- Amthauer, G., Annersten, H., and Hafner, S.S. (1976) The Mössbauer spectrum of  $^{57}\text{Fe}$  in silicate garnets. *Zeitschrift für Kristallographie*, 143, 14–55.
- Armbruster, T., and Geiger, C.A. (1993) Andradite crystal chemistry, dynamic X-site disorder, and structural strain in silicate garnets. *European Journal of Mineralogy*, 5, 59–71.
- Armbruster, T., Geiger, C.A., and Lager, G.A. (1992) Single crystal X-ray structure study of synthetic pyrope almandine garnets at 100 and 298 K. *American Mineralogist*, 77, 512–521.
- Bunau, O., and Joly, Y. (2009) Self-consistent aspects of X-ray absorption calculations. *Journal of Physics: Condensed Matter*, 21, 345501.
- Collerson, K.D., Williams, Q., Kamber, B.S., Omori, S., Arai, H., and Ohtani, E. (2010) Majoritic garnet: A new approach to pressure estimation of shock events in meteorites and the encapsulation of sub-lithospheric inclusions in diamond. *Geochimica et Cosmochimica Acta*, 74, 5939–5957.
- Frost, D.J., Poe, B.T., Tronnes, R.G., Liebske, C., Duba, A., and Rubie, D.C. (2004) A new large-volume multi-anvil system. *Physics of the Earth and Planetary Interiors*, 143–144, 507–514.
- Fursenko, B.A. (1981) Synthesis of new high pressure garnets:  $\text{Mn}_3\text{Cr}_2\text{Si}_3\text{O}_{12}$  and  $\text{Fe}_3\text{Cr}_2\text{Si}_3\text{O}_{12}$ . *Bulletin de Minéralogie*, 104, 418–422.
- Irfune, T. (1987) An experimental investigation of the pyroxene-garnet transformation in a pyrolyte composition and its bearing on the constitution of the mantle. *Physics of the Earth and Planetary Interiors*, 45, 324–336.
- Karpinskaya, T.B., Ostrovsky, I.A., and Yevstignejeva, T.L. (1982) Synthetic pure iron skiagite garnet. *Izvestia Akademii Nauk, SSSR*, 9, 128–129 (in Russian).
- Pascarelli, S., Mathon, O., Muñoz, M., Mairs, T., and Susini, J. (2006) Energy-dispersive absorption spectroscopy for hard-X-ray micro-XAS applications. *Journal of Synchrotron Radiation*, 13, 351–358.
- Petricek, V., Dusek, M., and Palatinus, L. (2014) Crystallographic computing system JANA2006: General features. *Zeitschrift für Kristallographie*, 229, 345–352.
- Potapkin, V., Chumakov, A.I., Smirnov, G.V., Celse, J.-P., Rüffer, R., McCammon, C., and Dubrovinsky, L. (2012) The  $^{57}\text{Fe}$  synchrotron Mössbauer source at the ESRF. *Journal of Synchrotron Radiation*, 19, 559–569.
- Prescher, C., McCammon, C., and Dubrovinsky, L. (2012) MossA: a program for analyzing energy-domain Mössbauer spectra from conventional and synchrotron sources. *Journal of Applied Crystallography*, 45, 329–331.
- Rehr, J.J., Kas, J.J., Prange, M.P., Sorini, A.P., Takimoto, Y., and Vila, F. (2009) Ab initio theory and calculations of X-ray spectra. *Comptes Rendus Physique*, 10, 548–559.
- Ringwood, A.E. (1975) *Composition and Petrology of the Earth's Mantle*, 618 p. McGraw Hill, New York.
- Rüffer, R., and Chumakov, A.I. (1996) Nuclear resonance beamline at ESRF. *Hyperfine Interactions*, 97–98, 589–604.
- Stachel, T. (2001) Diamonds from the asthenosphere and the transition zone. *European Journal of Mineralogy*, 13, 883–892.
- Sturhahn, W. (2000) CONUSS and PHOENIX: Evaluation of nuclear resonant scattering data. *Hyperfine Interactions*, 125, 149–172.
- Woodland, A.B., and O'Neill, H.St.C. (1993) Synthesis and stability of  $\text{Fe}^{2+}\text{Fe}^{3+}\text{Si}_2\text{O}_{12}$  garnet and phase relations with  $\text{Fe}_3\text{Al}_2\text{Si}_3\text{O}_{12}$ – $\text{Fe}_3^{2+}\text{Fe}^{3+}\text{Si}_3\text{O}_{12}$  solutions. *American Mineralogist*, 78, 1000–1013.
- (1995) Phase relations between  $\text{Ca}_3\text{Fe}^{2+}\text{Si}_3\text{O}_{12}$ – $\text{Fe}_3^{2+}\text{Fe}^{3+}\text{Si}_3\text{O}_{12}$  garnet and  $\text{CaFe}_2\text{Si}_2\text{O}_6$ – $\text{Fe}_2\text{Si}_2\text{O}_6$  pyroxene solid solutions. *Contributions to Mineralogy and Petrology*, 121, 87–98.
- Woodland, A.B., and Ross, C.R. II (1994) A crystallographic and Mössbauer spectroscopy study of  $\text{Fe}_3\text{Al}_2\text{Si}_3\text{O}_{12}$ – $\text{Fe}_3^{2+}\text{Fe}^{3+}\text{Si}_3\text{O}_{12}$  and  $\text{Ca}_3\text{Fe}^{2+}\text{Si}_3\text{O}_{12}$ – $\text{Fe}_3^{2+}\text{Fe}^{3+}\text{Si}_3\text{O}_{12}$  (andradite-skiagite) garnet solid solutions. *Physics and Chemistry of Minerals*, 21, 117–132.
- Woodland, A.B., Bauer, M., Boffa Ballaran, T., and Hanrahan, M. (2009) Crystal chemistry of  $\text{Fe}_3\text{Cr}_2\text{Si}_3\text{O}_{12}$ – $\text{Fe}_3\text{Fe}_2\text{Si}_3\text{O}_{12}$  garnet solid solutions and related spinels. *American Mineralogist*, 94, 359–366.

MANUSCRIPT RECEIVED DECEMBER 11, 2014

MANUSCRIPT ACCEPTED APRIL 25, 2015

MANUSCRIPT HANDLED BY OLIVER TSCHAUNER